Chinese Journal of Chemical Engineering 26 (2018) 1992–2002

Contents lists available at ScienceDirect

Chinese Journal of Chemical Engineering

journal homepage: www.elsevier.com/locate/CJChE

Article

Characterization and thrust measurements from electrolytic decomposition of ammonium dinitramide (ADN) based liquid monopropellant FLP-103 in MEMS thrusters☆

Asad Rahman [1], Jitkai Chin [1,*], Feroz Kabir [2], Yew Mun Hung [3]

[1] Department of Chemical and Environmental Engineering, University of Nottingham Malaysia Campus, Jalan Broga, 43500 Semenyih, Selangor, Malaysia
[2] Department of Engineering and Mathematics, Sheffield Hallam University, Sheffield S1 1WB, United Kingdom
[3] Department of Mechanical Engineering, Monash University Sunway Campus, Jalan Lagoon Selatan, 47500 Subang Jaya, Selangor, Malaysia

ARTICLE INFO

Article history:
Received 16 March 2017
Received in revised form 28 June 2017
Accepted 23 September 2017
Available online 16 October 2017

Keywords:
Ammonium Dinitramide (ADN)
FLP-103
Electrolytic decomposition
MEMS thruster

ABSTRACT

Although ammonium dinitramide (ADN) has been targeted as a potential green monopropellant in future space vehicles, its application potential in Micro-electrical–Mechanical System (MEMS) thrusters or microthrusters has been seldom reported in open literature. In this paper, electrolytic decomposition of Ammonium Dinitramide (ADN)-based liquid monopropellant FLP-103 was carried out in an open chamber and MEMS thrusters were fabricated from poly-dimethylsiloxane (PDMS) to characterize the power consumption. Two thrust measurement methods were employed to investigate the electrolytic decomposition of FLP-103 in MEMS microthrusters. The results show that the monopropellant can be successfully ignited at room temperature through 80 V, 0.1 A (8 W) using copper wire as electrodes. In the current thruster design, low thrust was obtained at FLP-103 flowrate of 40 $\mu l \cdot min^{-1}$ but it generated the highest specific impulse, *Isp*, among all the flowrates tested. The experiments successfully demonstrated the potential application of electrolytic decomposition of FLP-103 in MEMS thrusters.
© 2017 The Chemical Industry and Engineering Society of China, and Chemical Industry Press. All rights reserved.

1. Introduction

The rapid development of the micro-satellites has promoted MEMS thrusters as a low cost solution for a number of maneuvering requirements of satellites such as attitude control [1] and navigation [2] that increased flexibility and multiple power phases. These thrust requirements of the micro-satellites depend on their weight and on the type of maneuvering required which can be achieved by installation of an array of MEMS thrusters [2]. In general, MEMS thruster systems are divided into two categories — chemical and electrical propulsion systems. The chemical propulsion system is further divided into solid and liquid propellant systems such as cold gas, vaporizing liquid [3], bi-propellant [1], monopropellant [2] and composite solid fuels [4,5]. Liquid propellant-based MEMS thrusters offer variable thrust and multiple ignitions as compared to solid fuel-based MEMS thrusters. Ceramics, metals and silicon oxides are common fabrication materials for MEMS thrusters but opaque. Polydimethylsiloxane (PDMS) is normally used because it offers ease of fabrication, transparency [6] and wide range of material compatibility [7].

The propellant ignition in MEMS thrusters depends on the type of fuel. For example thermal heating is suitable for both liquid and solid fuels [8], while catalytic [9], spark and electrolytic ignition works only for liquid fuels. In a thermal conduction heating method, the propellant is heated to its decomposition temperature. However, higher thermal losses at micro-scale due to increased surface-to-volume ratio are undesirable [9]. Another disadvantage of conduction heating is its susceptibility to higher energy requirement compared to resistive heating where energy is supplied directly into the propellant [10]. The catalytic ignition has lower ignition temperature but is prone to loss of catalytic activity with repeated usage [2]. On the other hand, electrolytic ignition offers an attractive alternative to obtain ignition and subsequently propellant decomposition at relatively low temperature with minimal usage of input power. Electrolytic decomposition of ionic liquid mono-propellants can be considered as a hybrid of both chemical and electrical propulsion systems because of a passage of electric current through the ionic liquid fuel in combustion chamber resulting in electrolysis [7] and resistive heating [11] that decomposes ionic liquid fuel.

Conventional liquid fuel such as hypergolic fuels require separate pressurized vessels which ultimately increases the overall weight [8] and cold gas vaporizing gives very low impulse [12]. In this study, an ADN-based liquid monopropellant, FLP-103, consisting of ADN, water, methanol, and urea as stabilizer, was used in electrolytic decomposition in a MEMS thruster [10,13,14]. The FLP-103 offers better performance, stability [15] and environmental friendliness as compared to conventional

☆ Supported by the Project of Ministry of Science, Technology and Innovation, Malaysia (MOSTI) (No.04-02-12-SF0160).
* Corresponding author.
E-mail address: Jit-kai.chin@nottingham.edu.my (J. Chin).

https://doi.org/10.1016/j.cjche.2017.09.016
1004-9541/© 2017 The Chemical Industry and Engineering Society of China, and Chemical Industry Press. All rights reserved.

hydrazine or ammonium perchlorate propellants. Furthermore, less than 2 ms of electro-resistive ignition of ADN based mono-propellants at macro-scale indicated that, ADN based mono-propellants are conductive and can be used in micro-scale electrolytic ignition [11]. The ignition initiated by splitting of ADN into ammonium ion (NH_4^+) and dinitramide acid ($N_4H_4O_4$) followed by further protonation of the dinitramide acid into nitric acid (HNO_3) and nitrous oxide (N_2O) to proceed with the combustion of the propellant [16].

In this paper, electrolytic decomposition of FLP-103 was demonstrated in an open chamber and a MEMS thruster. Experiments in the open chambers were aimed to verify power usage and investigate any presence of solid residue after electrolytic decomposition of the liquid monopropellant. This latter case will have a significant influence on MEMS thruster design. The MEMS thruster used in this experiment is based on a well-established thruster design, in which gaseous product of the electrolytic decomposition of FLP-103 will be forced through a nozzle, in the MEMS thruster to generate thrust. Then, the work will focus on the electrolytic decomposition in MEMS and thrust measurement using a load cell and induction sensor respectively. Specific impulse, *Isp*, was compared.

2. Experimental

2.1. Preparation of FLP-103

The ADN synthesis was initiated by nitration of potassium sulfamate (H_2KNO_3S) with a mixture of nitric (HNO_3) and sulfuric acids (H_2SO_4) at −45 °C [17]. The FLP-103 was prepared by dissolving ADN in deionized water followed by addition of methanol and urea with the following composition: ADN 63.4 wt%, water 25.3 wt%, methanol 11.2 wt%, and urea 0.1 wt% [10,13,14]. The product was then analyzed in a Thermogravimetric Analyzer (Mettler Toledo) at a heating rate of 10 °C·min^{-1} in a nitrogen atmosphere. The flowrate of the nitrogen was 50 ml·min^{-1} to prevent unwanted oxidation.

2.2. Fabrication of open chamber

The experiment in open chambers was carried out to investigate the rate of reaction with respect to applied voltage. In the first step, premixed PDMS polymer was filled into a flat surfaced paper cup to obtain a 2–3 mm thick flat surface and cured. Next, thin glass microscope slides (local supplier) with dimensions of 100 mm length, 1 mm thickness, and 25 mm width were erected vertically into the cured PDMS flat surface followed by addition of more PDMS until a depth of 5–6 mm was achieved, and it was allowed to cure. Once PDMS was cured, the glass slides were removed to obtain several open chambers. Then each open chamber was separated by manual cutting, and used for experiment. The fabrication steps are shown in Fig. 1. The dimensions of the open-chamber were: 1 mm width, 25 mm length, and 5–6 mm height.

In the experiment, a ruler with 1 mm least count was placed behind the open chamber device for scaling and visualization purposes. Copper wires were used as electrodes at both sides and connected to a power supply. 100 µl FLP-103 was displaced into the open chamber and electrolysis of the propellant was initiated from DC power supply (Elektro Automatik) at 80 V 0.1 A. The experiment was repeated with various voltages of 5–80 V.

The entire electrolytic ignition phenomenon was recorded by an Asus camera (Asus, Z6) at HD resolution (1920 × 1080, 27 frames per second) for visual observation.

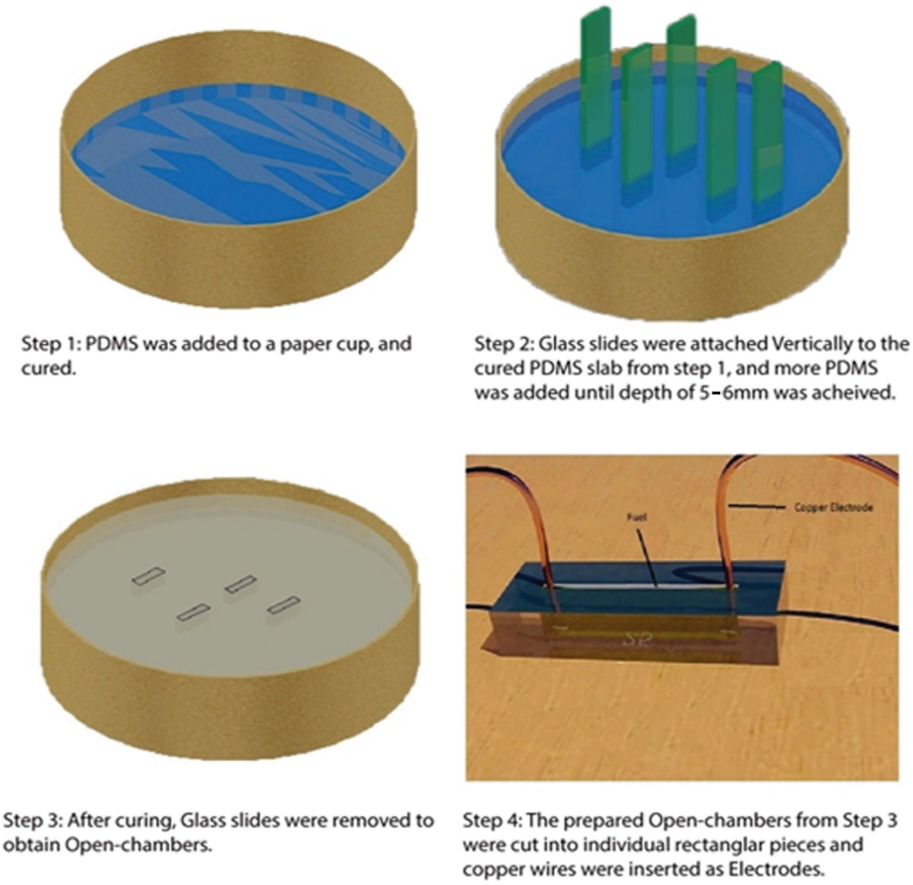


Fig. 1. Fabrication steps of open-chamber used for bubble size measurements (not to scale).

The video was analyzed frame by frame using a MATLAB Image Processing Tool. The images were converted in millimeter scale. At least 3 measurements for each video were calculated and averaged to estimate bubble diameter.

In this section, a well-established MEMS thruster design was used without optimization due to two reasons. First, there is a lack of open data for ADN mono-propellant specific optimized thruster specifications in micro-scale, especially under electrolytic conditions. Secondly, the section is aimed at studying the feasibility of electrolytic decomposition of FLP-103 in a MEMS thruster and hence for convenience and simplicity. The design of the MEMS thruster highly depends on the mass flow and ratio of the nozzle exit area to the nozzle throat area nozzle, also known as nozzle expansion ratio (Ae/At). The parameters determining the expansion of exhaust gas in a given exit pressure have been discussed [18] and the expansion ratio is 4 [19]. The throat diameter was selected as 250 μm due to the limitation of the xurographic fabrication method [20].

The thruster was designed and fabricated as a combination of engraving and embossing device, as shown in Fig. 2, this design is effective as both panels can interlock into each other to offer lateral support and prevent leakage. In order to eliminate backpressure and consequently thrust fluctuations, 90° bents were introduced between fuel injection and the combustion chamber. These thrust fluctuations could also be attributed to the flexibility of PDMS substrate and inconsistent fuel supply. The dimensions of the combustion chamber are elaborated in Fig. 3.

The MEMS thruster fabrication was performed *via* the xurographic method [20]. The thruster design was cut on a 200 μm thick 2-layer vinyl sheet laminated on a projector transparency sheet from a cutting plotter (Graphtec CE5000 plotter). The cutting plotter was programed to 23 N pressure and the slowest cutting rate to cut through the 2-layer vinyl sheet properly. Degassed PDMS mixture was then poured onto the laminated vinyl sheet and allowed to cure for 2 h at 60 °C. Both PDMS panels were then bonded to each other by applying a thin layer of tetrabutylammonium fluoride (TBAF) and cured for 2 h at 70 °C under pressure to obtain a uniform sealing. After sealing, a syringe needle and commercial copper wires (Element 14) were inserted at their respected locations as shown in Fig. 2. The use of copper wires as an effective electrode in electrolytic decomposition of hydroxyl ammonium nitrate (HAN), which is another ionic liquid propellant was demonstrated by [7]. FLP-103 was connected into the device from external storage *via* a syringe pump (KD Scientific, KDS-210). The graphical representation of the fabrication steps is shown in Fig. 4.

2.3. Experimental setup for thrust measurement

Experimental setup for the recording of thrust is shown in Fig. 5. The performance of the MEMS thrusters was characterized by two different thrust measurement methods — load cell and induction sensor respectively. The previous method is based on the momentum method in which the membrane of the force sensor vibrated due to thrust generated from the nozzle of the MEMS thruster, while the latter is based on correlation between the displacement of the balance arm of the measurement system due to thrust from the MEMS thruster and the current disturbance within the induction sensor. The thrust measurements obtained by the load cell and induction sensor is compared and analyzed.

2.3.1. Thrust measurement by load cell

The experiment was carried out using a miniaturized load cell (LSB200, Futek) placed at 1 mm and 2 mm from the exit nozzle of the MEMS thruster, horizontal with respect to the ground to avoid accumulation of condensed vapors, which is otherwise avoided by infrared heating of the sensor plate as demonstrated by [8]. In a horizontal arrangement, condensed gases from the burning fuel are accumulated on the sensor plate and disturb the data recording, therefore, infrared or other heating source is pointed at the sensor by means of optical focusing (magnifying glass) to immediately evaporate the condensing gases [8]. The distance of 2 mm from the thrust exit was considered small enough to represent actual thrust generated by thruster [1]. The distance between the thrust exit and sensor is a very important parameter, because the gases coming out of the thrust exit can start accumulating on the sensor as condensed vapor, and in the absence of this gap, the sensor detects the pressure from the fuel pump.

In addition, in the absence of this gap, the sensor detects the pressure from the fuel pump. Therefore, experiments were conducted to at both, 1 and 2 mm distance to identify the suitable distance for FLP-103. In the experiment, data was collected at a sampling rate of 100 Hz.

The specific impulse was calculated according to the Eq. (1).

$$Isp = \sum F \times \mathrm{d}T/\dot{m} \tag{1}$$

where, F, $\mathrm{d}T$ and $\dot{m}$ represent total force, time change and weight of total fuel respectively.

2.3.2. Thrust measurement by induction sensor

This system was designed and fabricated using off-the-shelf components. It was fabricated in-house using acrylic plastic sheets, PDMS, permanent magnets and an LDC1000 induction sensor (LDC-1000,

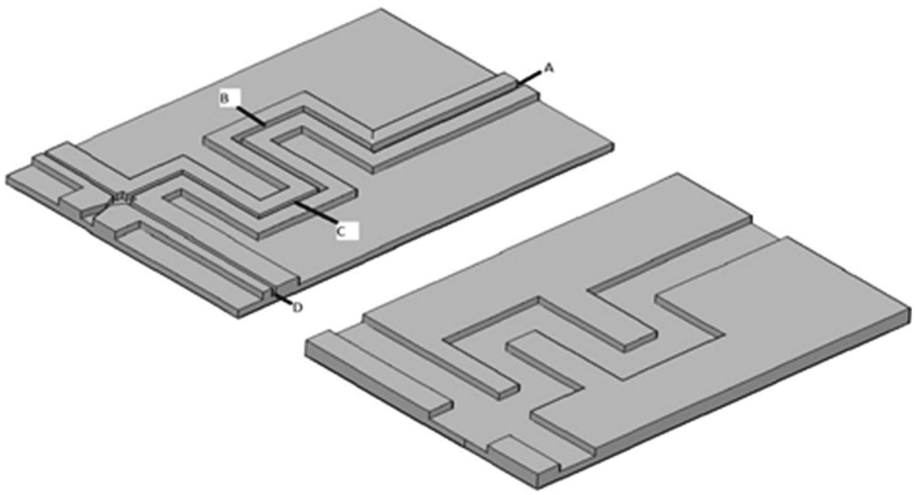


Fig. 2. AutoCAD rendered image of both sides of the actual thruster, channel width = A: 600 μm (location of needle insertion), B: 400 μm, C: 300 μm, D: 250 μm (location of copper wire insertion). The interlocking design offered ease of alignment and eliminated leakages.

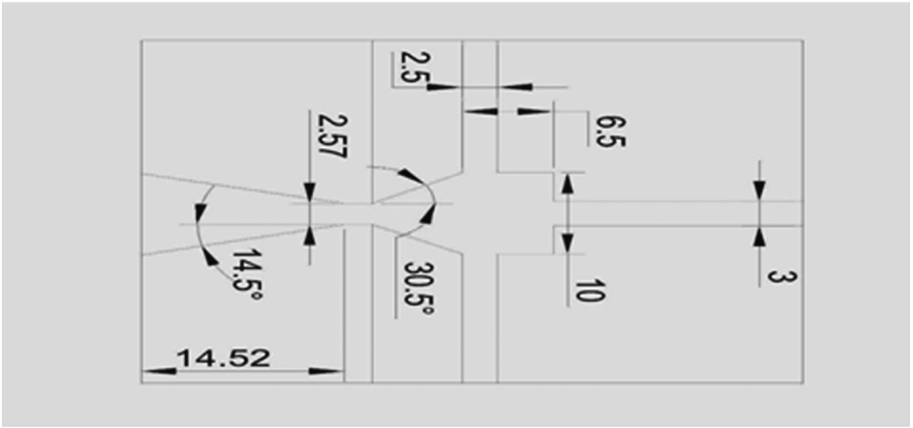


Fig. 3. Combustion chamber dimensions (scale: 1 = 100 μm).

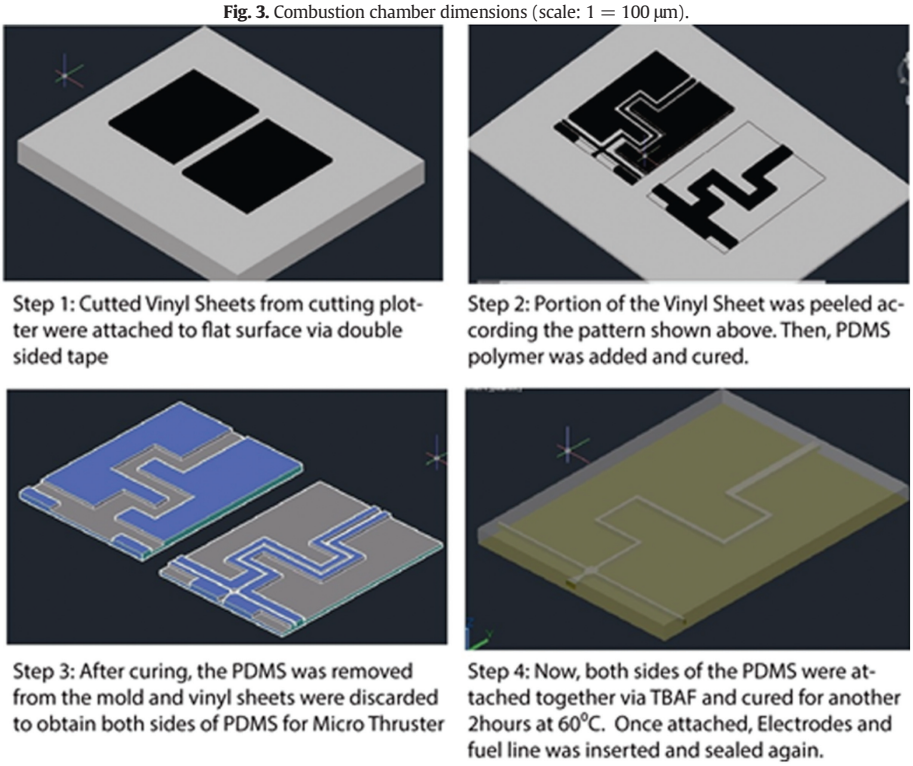


Fig. 4. Steps of PDMS MEMS thruster fabrication.

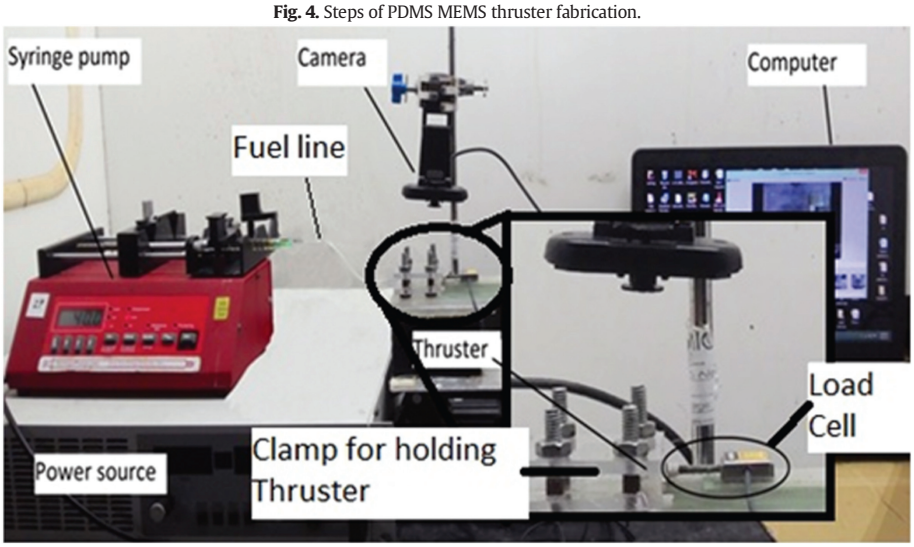


Fig. 5. Experimental setup used for thrust data recording.

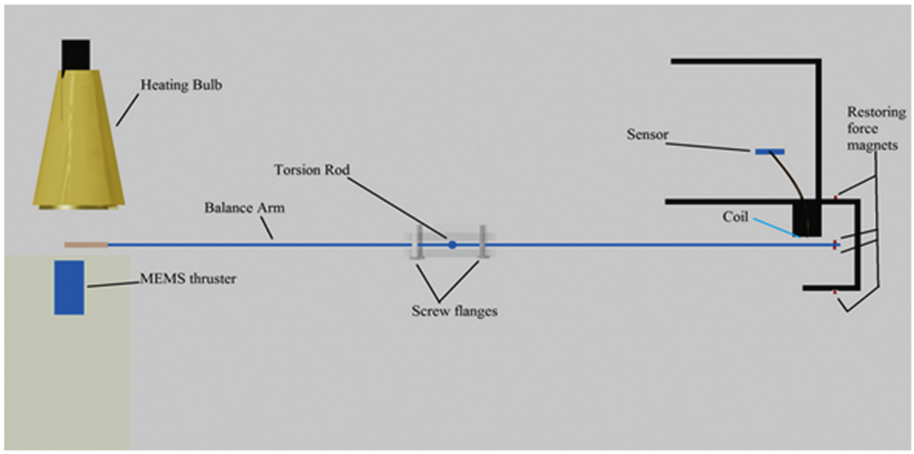


Fig. 6. AutoCAD generated top view of the thrust measurement system.

Texas Instruments, USA). The design concept of the thrust measurement by the induction sensor system is shown in Figs. 6 and 7. It was designed to demonstrate usage of PDMS as a fabrication material for torsional rod and to identify its potential application by comparing the results with the load cell system (Fig. 8).

The system comprised of an induction sensor with a default unit in micro-henry (μH) and a torsion rod. The torsion rod was molded in a 6 mm plastic pipe and 2600 mm × 30 mm × 1 mm aluminum plate as a balance arm, inserted into the center. The setup, as shown in detail in Fig. 9, was tightened by screw flanges while the edges were sealed with epoxy.

Then, the stand for restoring force magnet was attached to a side of the aluminum plate with the induction sensor. On the opposite side of the aluminum plate, the nozzle of the MEMS thruster was located at 2 mm from the aluminum plate and a 50 W halogen bulb was used as a point heating source to evaporate condensed vapors and un-burnt fuel.

The induction sensor was calibrated by pre-weighted aluminum chips into a weight tray attaching to the aluminum plate *via* string. The deflection of the aluminum plate by addition of pre-weighted aluminum chips was plotted for the linear relationship between the weights of aluminum chips to the displacement.

3. Results and Discussion

3.1. Analysis into decomposition of FLP-103 in open chamber

In Fig. 10, TGA–DSC analysis shows continuous and steady evaporation of FLP-103 observed until a sharp fall in mass at 166 °C. This result is corresponding to the decomposition of ADN, as reported in literatures, in the range of 140–170 °C [21,22].

There are three important assumptions in analysis into the electrolytic decomposition of FLP-103. First, the FLP-103 is assumed to gain heat uniformly up to ignition temperature, and ignition starts at the geometric center of propellant mass [23]. Secondly, the electrolytic decomposition products are in gas phase. Thirdly, the release of mass-dependent chemical energy at initial ignition heats up the combustion chamber but loses energy to the surroundings simultaneously. However, in the electrolytic ignition of ionic propellants such as FLP-103, the ignition occurs near the electrodes at a temperature lower than the decomposition temperature [10].

Therefore, tests were performed in open-chambers to identify dominating experimental parameters such as voltage and initiation of electrolysis.

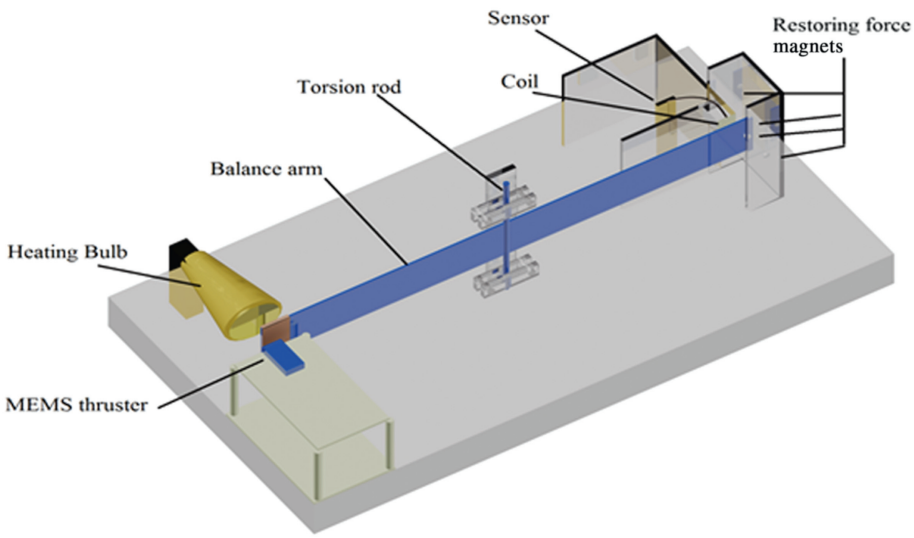


Fig. 7. Isometric view of the home made thrust stand. The balance arm is supported by a torsion rod. In experiment, the thruster is located at the left hand side while the restoring force and induction sensor are located at the right hand side. In experiment, thrust from the MEMS thruster causes small lateral displacements of the balance arm, resulting in current change within the sensor.

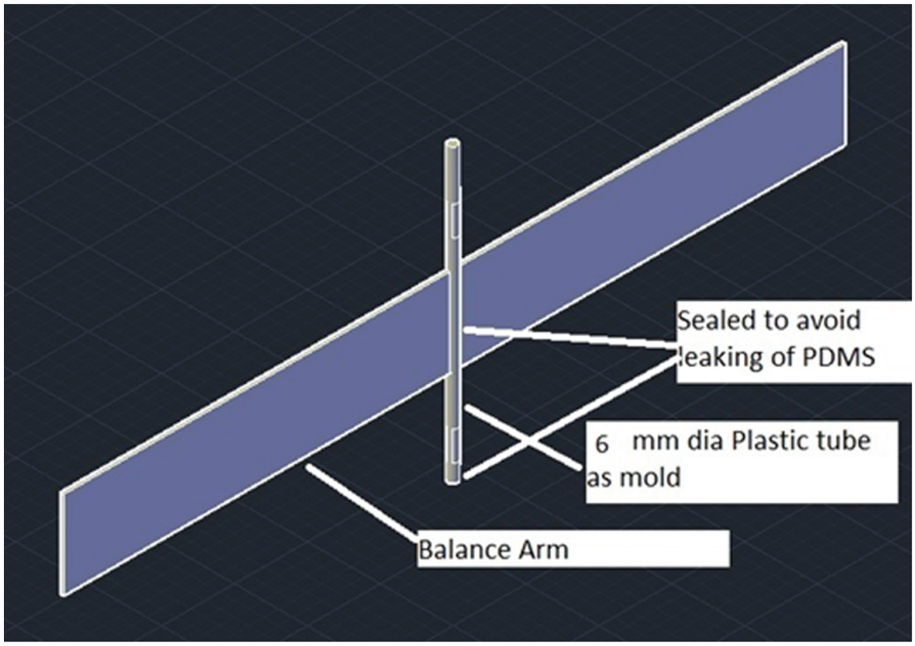


Fig. 8. Overview of PDMS based torsion rod fabrication.

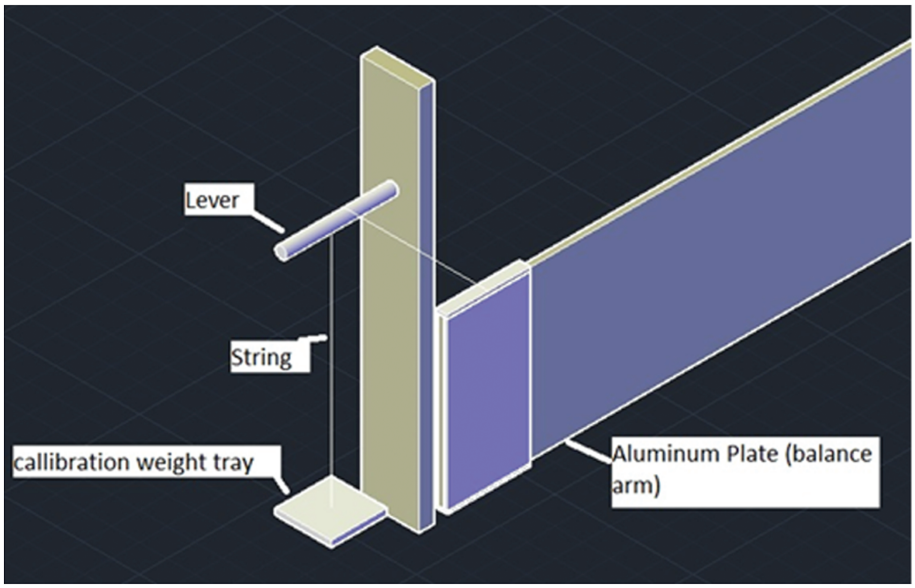


Fig. 9. Calibration of the thrust measurement method by induction sensor. Calibration weights were added in weight tray to record the movement generated by their pull on the aluminum plate. The calibration experiment was repeated with $R^2 = 0.9846$.

Before experiments in the MEMS thruster, an experiment was carried out to identify the optimum power consumption. A comparison of electrolysis at different voltages is shown in Fig. 11. At a fixed current of 0.1 A, 80 V generated the highest bubble areas within the chamber. The input setting of 5 V, 2 A (10 W) gave the lowest bubble area generation despite higher overall power wattage compared to 80 V, 0.1 A (8 W).

Fig. 12 shows electrolytic decomposition of FLP-13 immediately after power (80 V, 0.1 A) was switched on. Assuming electrolytic decomposition of FLP-103 produces only gaseous products, the bubble size growth was measured immediately after the first bubble appeared at the cathode. At the 3rd second, bubbles are visibly generated at the cathode rather than in the center of two electrodes. By the 5th second, the cathode had been completely surrounded by the bubbles. However, the bubble size increased continuously that by the 9th second, almost half of the space available inside the open chamber was taken by the gas bubbles, while bubble growth at the anode was extremely slow. A similar phenomenon was also noticed in electrolytic decomposition of hydroxyl ammonium nitrate (HAN) by [24].

Electrolytic decomposition of liquid monopropellant in a chamber and flow condition require separate characterization. In the latter case, flow dynamic causes fresh liquid propellant always surrounded the electrodes while gas bubbles will be pushed downstream. The investigation into input voltage in flow condition was carried out in MEMS thrusters at a propellant flow rate of 40 $\mu l \cdot min^{-1}$ and increments of 20 V at constant current 0.1 A. Decomposition was not noticeable at voltage below 40 V, with the propellant flow directly to the nozzle exit. Mild bubbling was noticed at 60 V but a plume of gases is visible

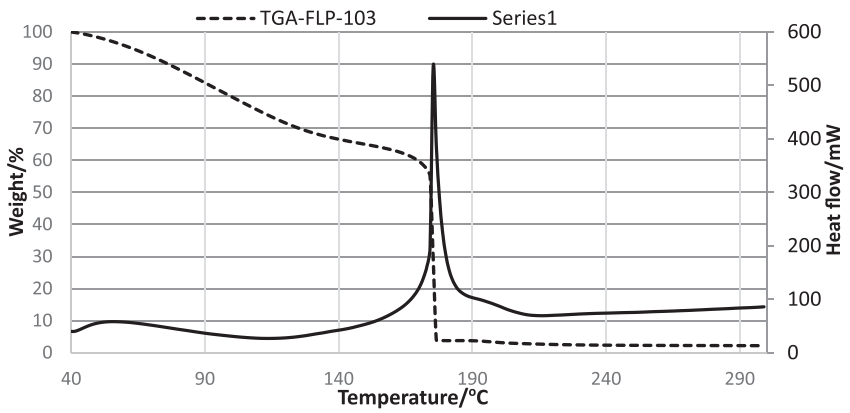


Fig. 10. DSC–TGA of FLP-103 obtained at heating rate of 10 °C·min^{-1}. The characterization examining weight loss (dotted line) and energy intake (solid line). Intercept between both lines indicating boiling point of the sample as the energy intake increases significantly enabling liquid boil-off.

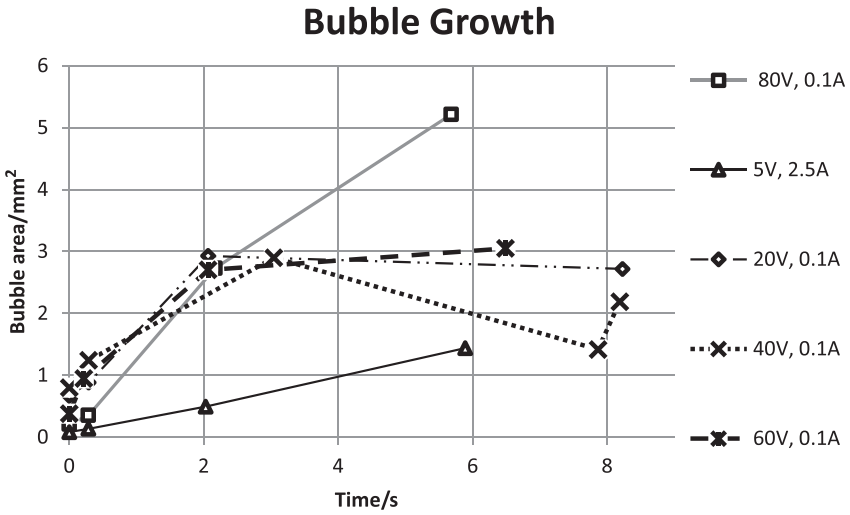


Fig. 11. Comparison of bubble growth in different power supplies shows that 80 V, 0.1 A produced bubbles more rapidly than all other settings. At 20, 40 and 60 V, the bubble generation slows down after reaching a peak.

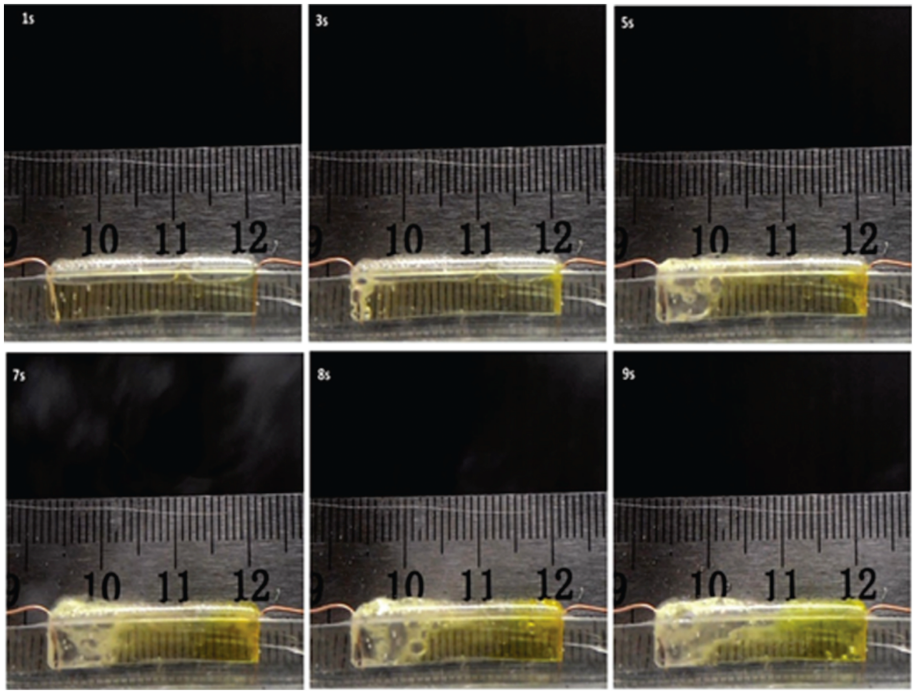


Fig. 12. Snapshots of electrolysis in open chamber taken at different intervals. The smoke and effervescence generation at the cathode (left) is noticeable.

Table 1
Observation of electrolytic decomposition of FLP-103 in MEMS thrusters at various flowrates and voltages. The current in all experiments was fixed at 0.1 A

Voltage/V	Propellant flowrates/μl·min^{-1}		
	40	60	80
20	Negative	Negative	Negative
40	Negative	Negative	Negative
60	Mild bubbling	Mild bubbling	Very mild bubbling and difficult to notice
80	Plume of exhaust gas from the nozzle	Plume of exhaust gas from the nozzle, occasionally with undecomposed FLP-103 at the nozzle	Plume of exhaust gas from the nozzle, few amount of undecomposed FLP-103 at the nozzle

at the nozzle exit at a flow rate of 80 V. The phenomena are summarized in Table 1.

3.2. Thrust measurement by load cell

Figs. 13, 14 and 15 show result of thrust measured from load cell located 2 mm from the nozzles of the MEMS thrusters, at flowrates of 40, 60 and 80 μl·min^{-1} respectively. Due to short residence time and hence longer contact time between the propellant and the electrodes, a flowrate of 40 μl·min^{-1} achieved steady state within 60 s but with the lowest thrust produced by all experiments.

The highest thrust was achieved at 80 μl·min^{-1} but the maximum specific impulse (*Isp*) was achieved at 40 μl·min^{-1}, as shown in Fig. 16. The low *Isp* obtained by 60 and 80 μl·min^{-1} flow rates was due to improper combustion in an undersized combustion chamber. In addition, thrust data collection for 80 μl·min^{-1} at 1 mm distance was unsuccessful due to interaction of undecomposed FLP-103 with the sensor.

The maximum experimental *Isp* obtained in this study is approximately 5 times less than the literature reported value 2492 N·s·kg^{-1} for ADN based propellants [23] in macro-thrusters. However, several factors contribute to low *Isp* of MEMS thrusters such as higher thermal losses [3], and low feed pressure [25] and most significantly, the reduced Reynold's number at micro-scale nozzles reduces the specific impulse up to 10 times [26]. The thermal losses are directly proportional to surface area, which explains the higher thermal losses at micro-level.

3.3. Thrust measurement by induction sensor

The thrust curves obtained by the induction sensor are shown in Figs. 17 and 18 for FLP-103 flowrates of 40 μl·min^{-1} and 60 μl·min^{-1} respectively. In this method, the flexural pivot works on the concept of bending of thin metal or plastic plates to provide movement without friction [27]. The induction sensor is more sensitive, hence able to detect lower thrust and lower *Isp* (Fig. 19) as compared to load cell (Table 2).

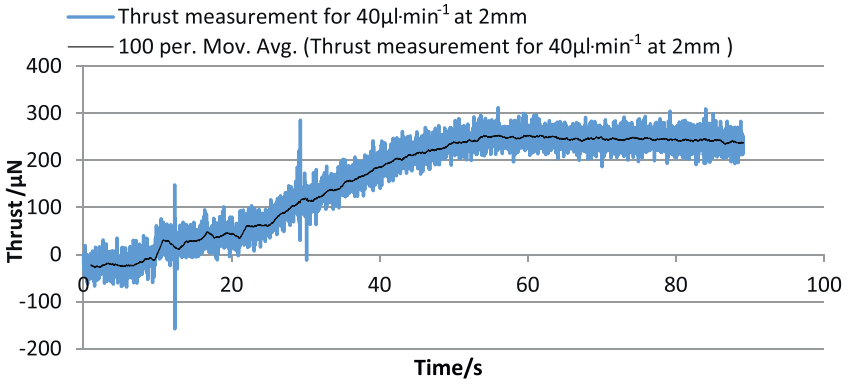


Fig. 13. Thrust measurement for 40 μl·min^{-1} propellant flowrate measured at 2 mm distance.

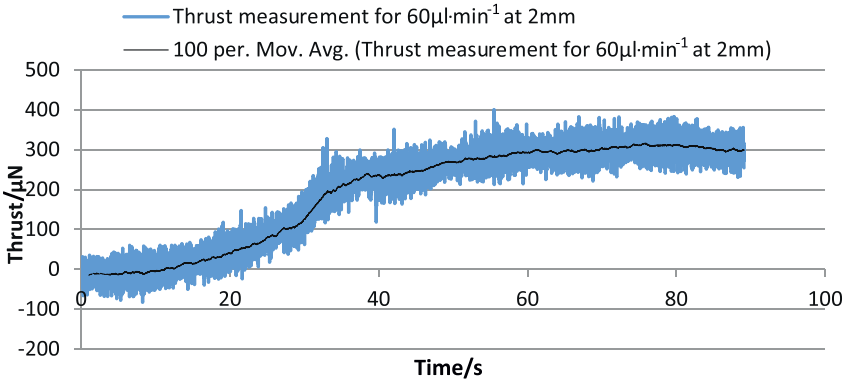


Fig. 14. Thrust measurement for 60 μl·min^{-1} propellant flowrate measured at 2 mm distance.

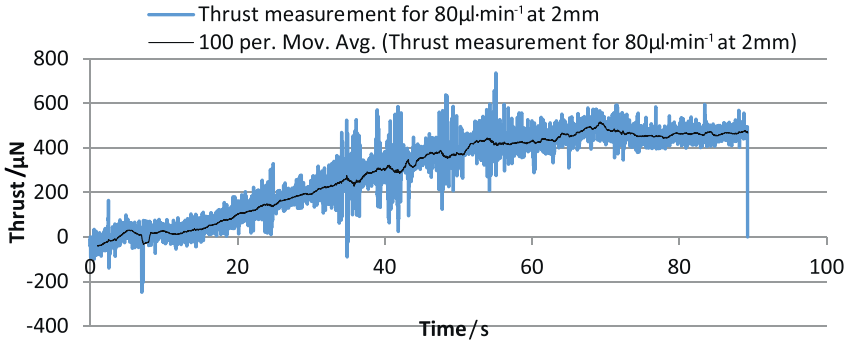


Fig. 15. Thrust measurement for 80 µl·min^{-1} propellant flowrate measured at 2 mm distance.

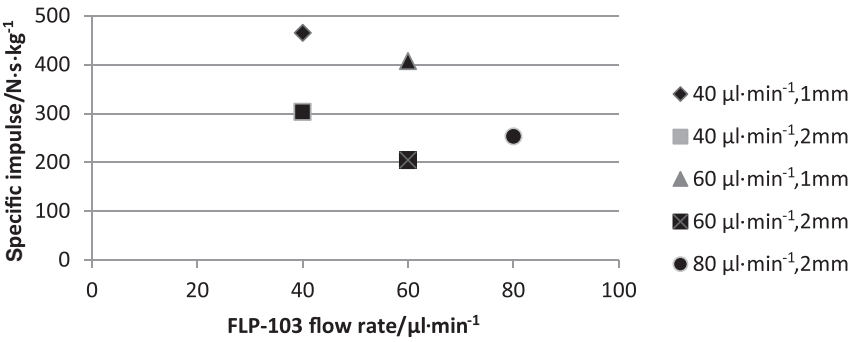


Fig. 16. Average specific impulse for different flowrates of FLP-103.

The differences between both thrust measurement methods were attributed to several factors. First, the calibration method used in the induction sensor was not frictionless. The friction coefficient induced between nylon thread and steel pulley is approximate to 0.36 μ_K [28], this may have caused reduced deflection in the aluminum plate. Secondly, the idle weights used during the calibration had an error up to 6 wt%. The error was calculated by weighting the aluminum strip before cutting into chips and comparing it with the sum of all the aluminum chips as shown in Table 3. From the experimental results shown in Fig. 14, it was evident that increasing distance between the thruster nozzle and sensor, which in this case is the aluminum plate, decreases the recorded thrust. In this experiment, thrust measurement by the induction sensor proves the feasibility of thrust detection *via* a PDMS based torsion rod in combination with an induction sensor.

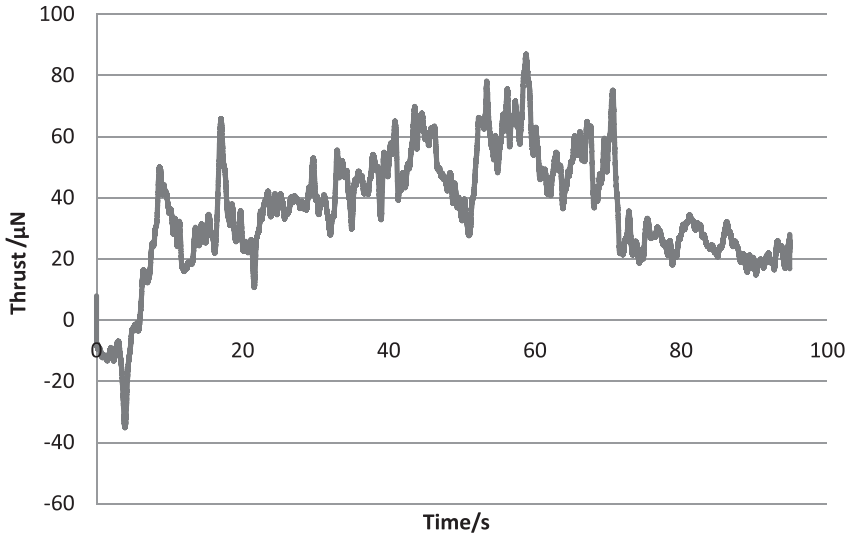


Fig. 17. Thrust measurement results for 40 µl·min^{-1} flowrate.

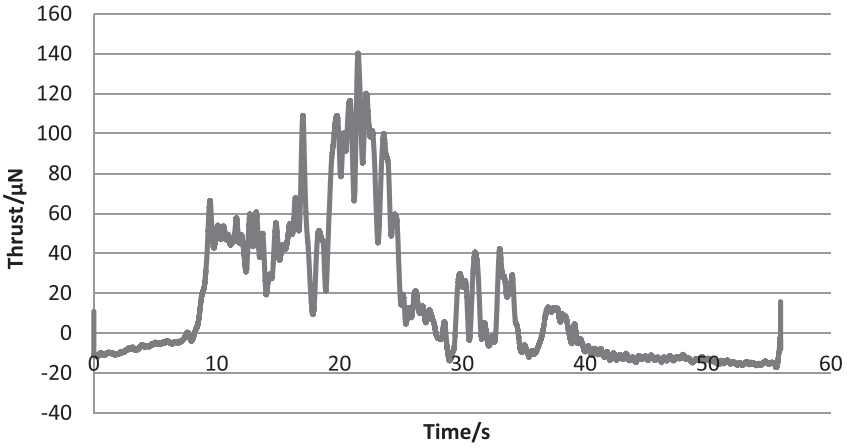


Fig. 18. Thrust measurement results for 60 μl·min^{-1} flowrate.

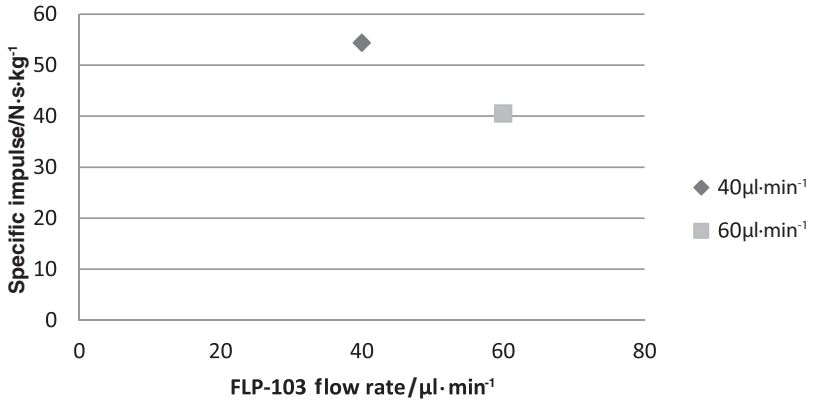


Fig. 19. Calculated specific impulse.

4. Conclusions and Future Works

In this paper, feasibility of electrolytic decomposition of Ammonium Dinitramide-based green liquid monopropellant, FLP-103, was successfully demonstrated in an open chamber and MEMS thrusters respectively, using an electrical setting of 80 V, 0.1 A (8 W). In open chamber devices, the reaction is mainly noticeable at cathode as the copper wire plays an important role in donating electrons throughout electrolysis. In flow experiments, 60 V, 01 A (6 W) only produced mild reaction within the MEMS thrusters in all tested flowrates. Although electrolytic decomposition at a flowrate of 40 μl·min^{-1} resulted in the lowest thrust, it produced the highest *Isp*. No back flow or leakage throughout the MEMS thruster experiments was observed, indicating appropriate thruster design selection and excellent xurographic fabrication method.

This paper also reported two low cost thrust measurement methods from electrolytic decomposition of FLP-103 from MEMS thrusters. In the first method, a force load cell measured the thrust directly at the nozzle of the thrusters, which is always inaccurate due to interaction of the load cell with unreacted propellant. The second method utilized an induction sensor, in which the measurement was carried out by the displacement of the balance arm in the measurement system.

Due to limited equipment available, the gaseous products of the electrolytic decomposition of FLP-103 were not collected and reaction kinetics were not analyzed in detailed. The work is currently being addressed to establish better understanding on the fundamental chemical reactions taking place. The theory is useful so as it can be used in designing MEMS thrusters specific for FLP-103 in the future.

Table 2
Comparison of specific impulse obtained from load cell and induction sensor

	Isp, 40 μl·min^{-1}/N·s·kg^{-1}	*Isp*, 60 μl·min^{-1}/N·s·kg^{-1}
Load cell (a)	300	200
Induction sensor (b)	54.3	40.48
Difference①	81.9%	79.76%

① $\frac{(a-b)\times 100}{a}\%$.

Table 3
Percentage error calculation in calibration weights (idle weights)

Total weight before cut	107.8 mg
Summed up weight of all Chips (after cutting)	101.5 mg
Difference	6.3 mg
Percentage of error	5.8%

References

[1] M.H. Wu, P.S. Lin, Design, fabrication and characterization of a low-temperature co-fired ceramic gaseous bi-propellant microthruster, *J. Micromech. Microeng.* 20 (8) (2010) 085026.

[2] J. Huh, K. Sejin, Design, fabrication and thrust measurement of a micro liquid mono-propellant thruster, *J. Micromech. Microeng.* 24 (10) (2014) 104001.

[3] K.H. Cheah, K.S. Low, Fabrication and performance evaluation of a high temperature co-fired ceramic vaporizing liquid microthruster, *J. Micromech. Microeng.* 25 (1) (2015) 015013.

[4] C. Rossi, B. Larangot, D. Lagrange, A. Chaalane, Final characterization of MEMS-based pyrotechnical microthruster, *Sensors Actuators A Phys.* 121 (2) (2005) 508–514.

[5] C. Ru, J. Dai, J. Xu, *et al.*, Design and optimization of micro-semiconductor bridge used for solid propellant microthrusters array, *Eur. Phys. J. Appl. Phys.* 74 (3) (2016) 30103.

[6] K. Takahashi, Contemporary Technology and Application of MEMS Rocket, 2006 (Toulouse, France).

[7] K.S. Koh, J. Chin, T.F. Chik, Role of electrodes in ambient electrolytic decomposition of hydroxylammonium nitrate (HAN) solutions, *Propuls. Power Res.* 3 (2) (2013) 194–200.

[8] P. Kundu, T.K. Bhattacharyya, S. Das, Design, fabrication and performance evaluation of a vaporizing liquid microthruster, *J. Micromech. Microeng.* 22 (2012) 025016.

[9] M.H. Wu, R.A. Yetter, A novel electrolytic ignition monopropellant microthruster based on low temperature co-fired ceramic tape technology, *Lab Chip* 9 (7) (2009) 910–916.

[10] A. Larsson, P. Appelgren, N. Wingborg, M. Elfsberg, Characterization and Electrical Ignition of ADN-based Liquid Monopropellants, Weapons and Protection, Swedish Defence Research Agency, 2005http://www.foi.se/ReportFiles/foir_1639.pdf.

[11] A. Larson, N. Wingborg, M. Elfsberg, P. Appelgren, Electrical Ignition of New Environmental-friendly Propellants for Rockets and Spacecrafts, 2005 497–500 (Monterey, CA).

[12] S.W. Janson, H. Helvajian, W.W. Hansen, J. Lodmell, Microthrusters for nanosatellites, The Second International Conference on Integrated Micro Nanotechnology for Space Applications, Pasadena, CA, 1999.

[13] K. Anflo, N. Wingborg, Ammonium Dinitramide Based Liquid Monopropellants Exhibiting Improved Combustion Stability and Storage Life, US0231765 A1, 2004.

[14] N. Wingborg, C. Eldsater, Henrik Skifs, Formulation and Characterization of ADN-based Liquid Monopropellants, 2004 (Cagliari, Sardinia, Italy).

[15] H. Matsunnaga, H. Habu, M. Atsumi, Thermal behavior of new oxidizer ammonium dinitramide, *J. Therm. Anal. Calorim.* 111 (2) (2012) 1183–1188.

[16] R. Yang, P. Thakre, V. Yang, Thermal decomposition and combustion of ammonium dinitramide (review), *Combust. Explosion Shock Waves* 41 (6) (2005) 657–679.

[17] G.H. Nazeri, R. Mastour, M. Fayaznia, P. Keyghobadi, Synthesis of ammonium dinitramide by nitration of potassium and ammonium sulfamate. The effect of sulfamate conterion on ADN purity, *Iran. J. Chem. Chem. Eng.* 27 (1) (2008) 85–89.

[18] K.L. Zhang, S.K. Chou, S.S. Ang, X.S. Tang, A MEMS-based solid propellant microthruster with Au/Ti igniter, *Sensors Actuators* 0041 (122) (2005) 113–123.

[19] N. Wingborg, M. Johansson, L. Bodin, Initial Development of a Laboratory Rocket Thruster for ADN-based Liquid Monopropellants, 2006 (Tumba).

[20] C.N. Lim, K.S. Koh, Y. Ren, *et al.*, Analysis of liquid–liquid droplets fission and encapsulation in single/two layer microfluidic devices fabricated by xurographic method, *Micromachines* 8 (2) (2017) 49/1–49/17.

[21] C. Kappenstein, Y. Batonneau, N. Wingborg, Non toxic ionic liquids as hydrazine substitutes. Comparison of physico-chemical properties and evaluation of ADN and HAN, 2nd Int. Conference of Green Propellants for Space Propulsion, Cagliari, Sardinia, Italy, 2004.

[22] S. Vyazovkin, C.A. Wight, Ammonium dinitramide: Kinetics and mechanism of thermal decomposition, *J. Phys. Chem.* 101 (1997) 5653–5658.

[23] P. Appelgren, A. Larsson, N. Wingborg, M. Elfsberg, Characterization and Electrical Ignition of ADN-based Liquid Monopropellants, Weapons and Protection, Swedish Defence Research Agency, 2005http://www.foi.se/ReportFiles/foir_1639.pdf.

[24] W.S. Chai, K.H. Cheah, K.S. Koh, J. Chin, T. Faraha, W.K. Chik, Parametric studies of electrolytic decomposition of hydroxylammonium nitrate (HAN) energetic ionic liquid in microreactor using image processing technique, *Chem. Eng. J.* 296 (July 2016) 19–27.

[25] K. Neff, P. King, K. Anflo, R. Mollerberg, High Performance Green Propellant for Satellite Applications, 4878, 2009 2–5 (Denver, Colorado).

[26] R.A. Yetter, V. Yang, M.-h. Wu, Y. Wang, D. Milius, I.A. Aksay, F.L. Dryer, Combustion issues and approaches for chemical microthrusters, *Int. J. Energetic Mater. Chem. Propul.* 6 (4) (2007) 393–424.

[27] B.D. Jensen, L.L. Howell, The modeling of cross-axis flexural pivots, *Mech. Mach. Theory* 37 (5) (2002) 461–476.

[28] P.J. Blau, Friction Science and Technology: From Concepts to Applications, Second edition CRC Press, 2008.